Alinejad, Farid; Bordbar, Hadi; Hostikka, Simo

The ordinate weighting method for solving radiative heat transfer through a Fresnel interface

Published in:
Journal of Quantitative Spectroscopy and Radiative Transfer

DOI:
10.1016/j.jqsrt.2021.107685

Published: 01/08/2021

Document Version
Publisher's PDF, also known as Version of record

Journal of Quantitative Spectroscopy & Radiative Transfer 270 (2021) 107685

Contents lists available at ScienceDirect

Journal of Quantitative Spectroscopy & Radiative Transfer

journal homepage: www.elsevier.com/locate/jqsrt

The ordinate weighting method for solving radiative heat transfer through a Fresnel interface

Farid Alinejad, Hadi Bordbar*, Simo Hostikka

School of Engineering, Aalto University, Finland

ARTICLE INFO

Article history:
Received 1 March 2021
Revised 16 April 2021
Accepted 16 April 2021
Available online 28 April 2021

Keywords:
Fresnel boundary
Ordinate weighting method (OWM)
Finite volume method
Radiation heat transfer
Refraction

ABSTRACT

Refraction of electromagnetic waves at Fresnel interfaces, i.e. the boundaries between media with different refractive indices, is important not only in explaining many natural phenomena but also in radiation heat transfer in energy conversion and combustion systems, such as solar energy, spray cooling and combustion, and the evaporation of liquid fuels in pool fires. This paper presents a novel model for the efficient consideration of Fresnel interfaces in the Finite Volume Method-based solvers of thermal radiation. By conserving the transmitted radiative heat flux at the Fresnel interface, the new model accurately estimates the directional distribution of radiative intensities on the second side of the interface. To do so, a matrix of weighting coefficients is obtained, representing the transferred radiation energy from the control angles on the first side of the Fresnel interface into each control angle on the second side. To assess the accuracy of the novel ordinate weighting method (OWM), its predictions are compared with the analytical solutions that we obtained for one- and two-layer slabs with various combinations of absorption and scattering properties. The validations are shown for normalized heat flux and irradiation, reflectivity, transmissivity, and intensity. The predictions of the OWM show an excellent agreement with the results of the analytical solutions. Compared to Murthy's pixelation method, the OWM method provides better accuracy with lower computational cost. Finally, the sensitivity of the OWM method to uniform and non-uniform directional discretizations, used in the finite volume solution of the radiative heat transfer, is investigated.

1. Introduction

Modeling spectral and directional dependency of radiative heat transfer in participating media has received substantial attention during the last few decades. Several models such as full spectrum correlated-k distribution (FSCK) [1,2], spectral line-based sum of gray gases (SLW) [3,4], and weighted sum of gray gases (WSGG) [5–8] have been developed to solve the spectral dependency of radiation intensity and some models like discrete ordinates method (DOM) [9,10], finite volume method (FVM) [11,12], zone method [14,15] and spherical harmonics method (SP) [13,16] have been proposed to solve its spatial and directional dependency. Most of these efforts focused on solving radiation heat transfer in the gas phase alone with only a few for the other phases [17,18]. However, in many applications such as fire dynamics modeling, remote sensing [19], solid-state lighting [20], solar applications [21], biomedical engineering [22], determining the radiative properties of the materials [23], optical fiber drawing process [24], and penetration of short-pulse lasers within participating media in different emerging applications [25], radiation transfer should be solved in multi-phase systems. In this kind of problems, radiation heat transfer should be modeled not only within the individual phases but also through the interface of different phases or materials. When an electromagnetic wave hits the interface of two media with different refractive indexes, a part of the irradiation is transmitted into the second medium and the rest is reflected [26]. Due to the difference in refractive indexes of the phases or materials, an important phenomenon of refraction occurs at the interface of the different phases altering the magnitude and directional distribution of the radiation intensity. The direction of intensity is given by Snell's law and the reflected share of the incident radiation is determined by applying the Fresnel relation [26]. In addition, within the optically dense side of the interface, radiation intensity with angles greater than a critical angle is completely reflected. In this paper, we use the term of Fresnel interface to refer to an interface that applies the aforementioned effects.

To numerically solve the radiation heat transfer through a Fresnel interface, a specific boundary condition should be applied

* Corresponding author.
E-mail address: hadi.bordbar@aalto.fi (H. Bordbar).

https://doi.org/10.1016/j.jqsrt.2021.107685

Nomenclature

Latin

$\tilde{a}$	Coefficient of linear anisotropic scattering
C	Coefficients of phase function series
D	Integral of direction vector over solid angle
d	Layer thickness (m)
G	Irradiation (W/m^2)
I	Intensity ($W/m^2/sr$)
I'	Redistributed intensity ($W/m^2/sr$)
I^+	Forward intensity ($W/m^2/sr$)
I^-	Backward intensity ($W/m^2/sr$)
I_b	Blackbody intensity ($W/m^2/sr$)
I_d	Diffuse intensity ($W/m^2/sr$)
I_{f1}	Intensity at upper face of a control volume ($W/m^2/sr$)
I_{f2}	Intensity at bottom face of a control volume ($W/m^2/sr$)
n	Refraction index
$\hat{n}$	Unit normal vector
P	Legendre polynomial
$\dot{q}''$	Heat flux (W/m^2)
$\dot{q}'''$	Heat source (W/m^3)
R	Reflection at a interface
r	Weighting parameter
S	Source term ($W/m^2/sr$)
$\hat{s}$	Direction vector
T	Tranmission through a layer
x	Location (m)

Greek

β	Extinction coefficient (m^{-1})
$\delta\Phi$	Averaged relative error of Φ
θ	Polar angle
κ	Absorption coefficient (m^{-1})
μ	Cosine of the polar angle
ρ	Reflectivity
$\tilde{\rho}$	Averaged reflectivity
σ_s	Scattering coefficient (m^{-1})
τ	Optical thickness
ϕ	Scattering phase function
$\tilde{\phi}$	Averaged scattering phase function
ψ	Azimuthal angle
Ω	Solid angle

Abbreviation

CDOM	Composite discrete ordinate method
DOM	Discrete ordinate method
FVM	Finite volume method
OWM	Ordinate weighting method
RTE	Radiative transfer equation

for directional redistribution of intensity. Despite the well-known theoretical concept and the vital importance of refraction at the boundary, a common approach for solving the radiation at a Fresnel interface is to assume directionally diffuse boundary, which effectively conserves radiating energy but neglects the difference between the refractive indices and consequently the directional dependency of radiation. Hence, some inaccuracy can be expected in the predicted reflectivity and radiative source terms when such an assumption is made.

Among the angular discretization methods, the two-flux method is the simplest one that considers two hemispheres in the forward and backward directions as two control angles. To consider a Fresnel boundary within this method, Dombrovsky et al. [27] developed a modified two-flux method which considers the transmitted radiation only within the angular region that is enclosed by a critical angle. Liou and Wu [28] included the Fresnel boundary in the composite discrete ordinates method (CDOM) by defining the discrete ordinates according to the direction of the transmitted radiation at both sides of the interface. For the modified discrete ordinates, a set of new ordinates' weights should be recalculated for each direction. However, in most of the radiation simulations using the DOM for different media, a set of fixed discrete ordinates is conventionally used, and the radiative transfer equation is discretized for each ordinate. By applying the CDOM, different sets of ordinates are used at each side of the interface. This procedure complicates the programming of the method. One of the aims of the present work is to avoid changing the angular discretization at the interface of two media, therefore a single set of ordinates would be applied to both phases. In another version of DOM, Zhang et al. [29] presented the radial basis function interpolation approach to find the refracted intensities at certain discrete angles in a multi-layer cylindrical medium. This interpolation is only done for polar angle within a plane that is defined by azimuthal angle. Similarly, Wei et al. [30] applied the radial basis function interpolation approach to find the refracted intensities at each specific control angle. For doing this interpolation, they have applied two different schemes: forward and backward interpolations. In the forward scheme, the interpolation is done for the refracted intensities, while, in the backward scheme, this interpolation is done before refraction. Their simulations showed that the former one is less stable when the ray propagates from an optically dense to an optically rarer medium. In this approach, the level of matching between the radial basis function and angular distribution of the intensity governs the accuracy. Therefore, the selection of the radial basis function is case dependent and can be a potential source of error. In another work, Zhang et al. [31] applied the DOM with interpolation in their analysis of radiative heat transfer in a two-dimensional semitransparent medium with a piece-wise constant refractive index. They used a simple linear interpolation to find the magnitude of the intensities at the locations of discrete ordinates. For the collimated incident radiation, Le Hardy et al. [32] applied the DOM for the angular discretization and expressed the incident term in the boundary condition of each discrete ordinate by proposing a repartitioning scheme that divides the incident term between two adjacent ordinates. The repartitioning is done by defining a shared coefficient which is calculated from the angles of refracted intensities of two adjacent ordinates. Although this method works well for collimated incident radiation, it cannot be generally accurate when the refracted incident radiation for an ordinate may occupy more than two ordinates at the other side of the boundary.

As reviewed, most numerical works considering Fresnel interfaces were based on DOM. Similar to DOM, modeling a Fresnel interface with FVM needs an additional effort to solve the mismatch of directional radiative intensity on two sides of the interface. Considering the Fresnel boundary introduces a misalignment between the angles of the transmitted intensities of each control angle as already explained. Murthy and Mathur [33] introduced two approaches to solve the issue of misalignment of direction of intensity in FVM. In their first approach, the correspondent centroid direction of each control angle is determined after passing the interface. Then, the whole radiation energy of that control angle is devoted to the control angle at the other side of the interface in which the correspondent centroid is located. This approach guarantees the conservation of radiative energy but it does not keep the directional distribution. In the second approach, they have applied the pixelation method to specify which part of the transmitted radiative energy is inside of any specific control angle at the second side of the interface. This approach gives

higher accuracy but with the cost of high computational time as a large number of pixels should be considered within each control angle.

In the present work, to improve the accuracy and computational performance of FVM in simulating the Fresnel interface, a new approach is presented that uses the same control angles on both sides of the Fresnel interface. To estimate the directional distribution of intensity after passing the interface, a weighting parameter matrix is calculated by conserving radiative heat flux at the interface.

This paper has been organized as follows. Reviewing the FVM solution of RTE, we will present the theoretical base of the new weighting approach in simulating a Fresnel interface within FVM in the next section. It will be followed by introducing the validation case studies and presenting general solutions for directional radiative intensity in one- and two-layer slabs. Section 4 presents the analytical and numerical results of the case studies. Finally, Section 5 summarizes the new contributions and conclusions of the present research work.

2. Model description

2.1. Finite volume method

To solve radiation heat transfer, the radiative intensity field in different directions should be obtained. The variation of intensity of each direction is determined by solving the radiative transfer equation:

$$\frac{dI}{ds} = \kappa n^2 I_b - \beta I + \frac{\sigma_s}{4\pi}\int_{4\pi} I(\hat{s}_i)\phi(\hat{s},\hat{s}_i)d\Omega_i \tag{1}$$

In the above equation, the parameters I, κ, σ_s and $\hat{s}$ are radiation intensity, absorption coefficient, scattering coefficient, and direction vector, respectively. The term $\phi(\hat{s},\hat{s}_i)$ is scattering phase function and the parameter β is extinction coefficient defined as $\beta = \kappa + \sigma_s$. Depending on the characteristics of the medium, different options for the scattering phase function can be considered. In this paper, we apply different forms of the phase function including isotropic phase functions, linear and non-linear anisotropic phase functions. Generally, the phase functions are described using the Legendre polynomials:

$$\phi(\hat{s},\hat{s}') = \phi(\mu_0) = \sum_{m=0}^{N} C_m P_m(\mu_0) \tag{2}$$

where μ_0 is the cosine of the angle between the incoming ray and the scattered ray. This parameter is defined as [34]:

$$\mu_0 = \mu\mu' + (1-\mu^2)^{\frac{1}{2}}(1-\mu'^2)^{\frac{1}{2}}cos(\psi-\psi') \tag{3}$$

In the above equation, ψ shows the azimuthal angle, and prime represents the scattered ray. If the phase function is not dependent on the azimuthal angle, the angle μ_0 will be equal to $\mu\mu'$ which is the case in the present research. In the case of linear anisotropic scattering, only the first two terms of Eq. (2) are considered [34,35]:

$$\phi(\mu_0) = 1 + \bar{a}\mu\mu' \tag{4}$$

where the coefficient $\bar{a}$ is given as:

$$\bar{a} = \sum_{m=0}^{\infty} \frac{(-1)^m a_{2m+1}(2m)!}{2^{2m}m!(m+1)!} \tag{5}$$

For the nonlinear anisotropic scattering, different phase functions can be considered depending on the medium. For the study of nonlinear scattering, a phase function with strongly backward scattering will be used [36]:

$$\phi(\mu_0) = 0.75 - 1.2\mu\mu' + 0.75\mu^2\mu'^2 \tag{6}$$

To solve the RTE, we use FVM in a one-dimensional test case (Fig. 1), but the method is equally applicable for two- and three-dimensional geometries. The details of the FVM discretization can be found in [37], leading to a discrete form of the RTE:

$$I_{p,i} = \frac{S_{pi}\Delta x\Delta\Omega_i - I_{f1,i}D_{f1,i} - I_{f2,i}D_{f2,i}}{\left(\beta - \frac{\sigma_s}{4\pi}\bar{\phi}_{ii}\right)\Delta x\Delta\Omega_i} \tag{7}$$

To derive this equation, a step discretization scheme has been applied for the estimation of the intensities at cell faces. In Eq. (7), $I_{p,i}$, $I_{f1,i}$, and $I_{f2,i}$ stand for the intensities at the node p, the upper and the bottom faces of the control volume p in the direction i as shown in Fig. 1. In addition, Δx is the grid size, and $\Delta\Omega_i$ is the corresponding solid angle for the considered control angle i. Finally, the parameter $D_{fj,i}$ is defined for the faces of the control volume ($j = 1, 2$) using the following equation:

$$D_{fj,i} = \int_{\Delta\Omega_i} \hat{s}_i.\hat{n}_j\, d\Omega \tag{8}$$

where $\hat{n}_j$ is the unit normal vector of the faces of each control volume. In Eq. (7), subscripts 1 and 2 for the parameter D represent the upper and bottom faces of the control volume p. Neglecting the first term on the right-hand-side of Eq. (1) (i.e. medium emission), the source term S_{pi} becomes

$$S_{pi} = \frac{\sigma_s}{4\pi}\sum_{\substack{j=1\\ j\neq i}}^{n} I_{p,j}\bar{\phi}_{ji}\Delta\Omega_j \tag{9}$$

where the parameter $\bar{\phi}_{ji}$ is calculated as

$$\bar{\phi}_{ji} = \frac{1}{\Delta\Omega_i\Delta\Omega_j}\int_{\Delta\Omega_i}\int_{\Delta\Omega_j}\phi(\hat{s}_i,\hat{s}_j)d\Omega_j d\Omega_i. \tag{10}$$

For the purpose of decreasing the number of needed iterations for convergence, the scattering term in direction i has been excluded from the summation term in Eq. (9) as recommended by Chai et al. [38].

2.2. Ordinate weighting method (OWM)

Different refractive indexes alter direction and magnitude of the intensity while passing the interface of two media as shown in Fig. 2. In FVM, a fixed angular discretization is considered and a constant intensity is assumed within each control angle. Change in the direction of intensity due to different refractive indexes of two adjacent media causes a misalignment problem in applying the standard form of FVM as shown in Fig. 3.

To apply a single solid angle discretization scheme in the FVM solution at both sides of the interface, we need a method to account for the interface without losing accuracy or increasing computational time. Applying the conservation of heat flux at the interface as discussed in Appendix A, the following equation is obtained:

$$n_a^2 D_a = n_b^2 D_b \tag{11}$$

where the parameters n_a and n_b are the refractive indexes of media a and b, respectively, and D_a and D_b are the corresponding values of the cell face angular integral (Eq. (8)). The calculation uses the Snell's law that gives the change of direction of the intensity at the interface as

$$\frac{\sin(\theta_a)}{\sin(\theta_b)} = \frac{n_b}{n_a} \tag{12}$$

Eq. (11) shows the conservation of the parameter n^2D for the intensities within each control angle at the interface. However, the parameter $n^2\Delta\Omega$ which is related to the irradiation does not conserve at the interface. Therefore, unlike the heat flux, the value of

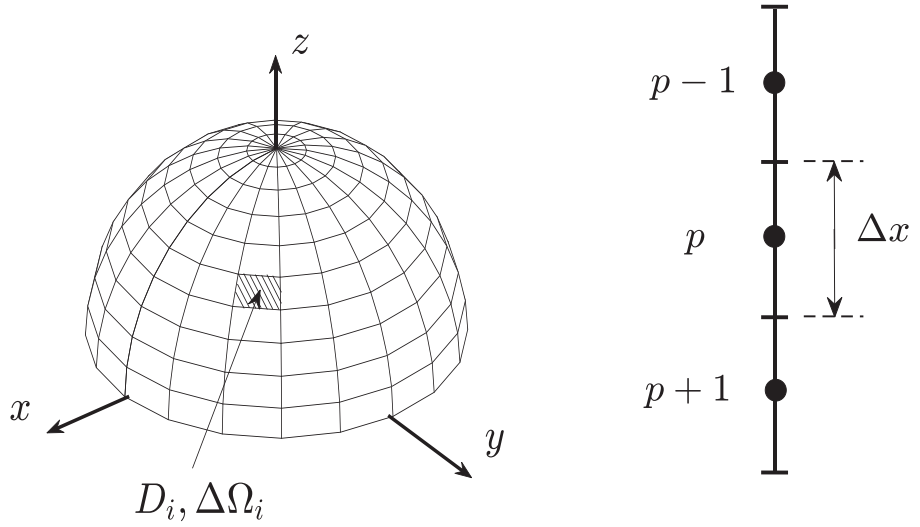

Fig. 1. Considered angular (left) and spatial (right) discretization for finite volume method.

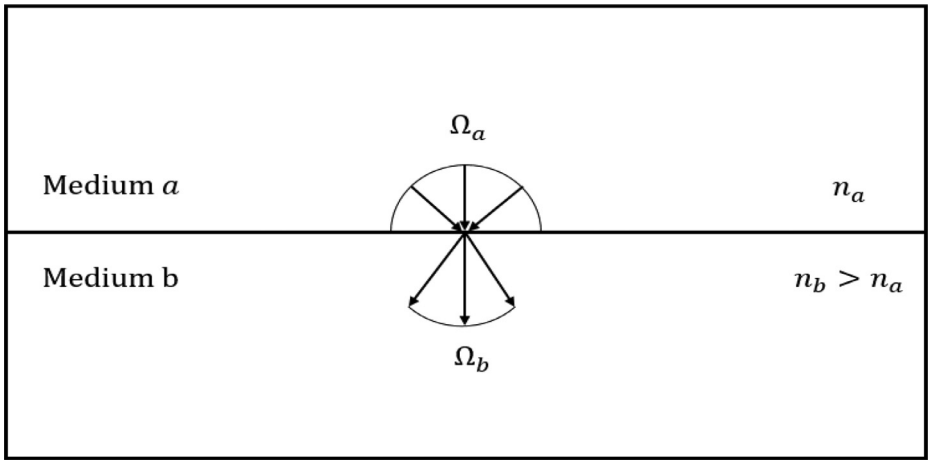

Fig. 2. Change of solid angle at the interface of two media with different refractive indexes.

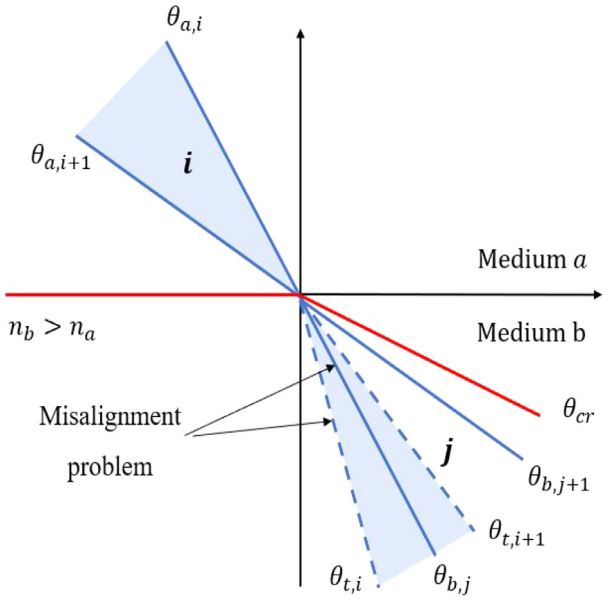

Fig. 3. Misalignment of transmitted intensities with the boundaries of the considered control angles for the finite volume method.

irradiation changes at the interface. Considering symmetric angular discretization with respect to the normal vector of the interface, the problem of misalignment is solved for reflection. Therefore, following this approach, the focus of this paper is to solve the misalignment problem of transmitted intensities.

Next, we consider the intensity within an arbitrary control angle i in the medium a as shown in Fig. 3 which has a corresponding angular span between the angles $\theta_{t,i}$ and $\theta_{t,i+1}$ in the medium b. As Fig. 3 shows, this angular span does not coincide with the control angle j in the medium b and covers only a part of it. For the control angle j, the radiative heat flux is calculated by the following integral equation:

$$\dot{q}''_{b,j} = \int_{\Delta\psi}\int_{\theta_{b,j}}^{\theta_{b,j+1}} I(1-\rho_{ab}(\theta_a))\left(\frac{n_b}{n_a}\right)^2 \cos(\theta_b)\sin(\theta_b)d\theta d\psi \quad (13)$$

where the parameter $\rho_{ab}(\theta_a)$ is the reflectivity of the interface at θ_a that is calculated using the Fresnel relation as [26]:

$$\rho_{ab} = \frac{1}{2}\left[\left(\frac{n_a\cos(\theta_b) - n_b\cos(\theta_a)}{n_a\cos(\theta_b) + n_b\cos(\theta_a)}\right)^2 + \left(\frac{n_a\cos(\theta_a) - n_b\cos(\theta_b)}{n_a\cos(\theta_a) + n_b\cos(\theta_b)}\right)^2\right] \quad (14)$$

The transmitted part of the radiative heat flux of the control angle j within the medium b comes from different control angles of the medium a. To calculate this heat flux, the misalignment of

the angular span between control angle j and transmitted heat flux from each control angles of medium a should be included in the heat flux equation:

$$\dot{q}'_{a,i\to j} = \int_{\Delta\psi}\int_{\max(\theta_{b,j},\theta_{t,i})}^{\min(\theta_{b,j+1},\theta_{t,i+1})} I_i(1-\rho_{ab}(\theta_a))\left(\frac{n_b}{n_a}\right)^2 \cos(\theta_b)\sin(\theta_b)d\theta d\psi \tag{15}$$

where $\max(\theta_{b,j},\theta_{t,i})$ and $\min(\theta_{b,j+1},\theta_{t,i+1})$ are the bounds of the misaligned angular span in medium b as shown in Fig. 3, and $\dot{q}''_{a,i\to j}$ is the transmitted heat flux from control angle i to control angle j. To enable a fixed solid angle discretization scheme in FVM, this heat flux should be distributed into the entire control angle j. To conserve the radiative heat flux, we introduce a redistributed intensity I':

$$\begin{aligned}&\int_{\Delta\psi}\int_{\max(\theta_{b,j},\theta_{t,i})}^{\min(\theta_{b,j+1},\theta_{t,i+1})} I_i(1-\rho_{ab}(\theta_a))\left(\frac{n_b}{n_a}\right)^2\cos(\theta_b)\sin(\theta_b)d\theta_b d\psi\\ &=\int_{\Delta\psi}\int_{\theta_{b,j}}^{\theta_{b,j+1}} I'(1-\rho_{ab}(\theta_a))\left(\frac{n_b}{n_a}\right)^2\cos(\theta_b)\sin(\theta_b)d\theta_b d\psi\end{aligned} \tag{16}$$

Now, the fraction of two intensities I' and I_i in Eq. (16) defines the weighting parameter r_{ji} as:

$$r_{ji} = \frac{I'}{I_i} = \frac{\int_{\max(\theta_{b,j},\theta_{t,i})}^{\min(\theta_{b,j+1},\theta_{t,i+1})}(1-\rho_{ab}(\theta_a))\cos(\theta_b)\sin(\theta_b)d\theta_b}{\int_{\theta_{b,j}}^{\theta_{b,j+1}}(1-\rho_{ab}(\theta_a))\cos(\theta_b)\sin(\theta_b)d\theta_b} \tag{17}$$

The main issue in estimation of r_{ji} is the difficulty of calculating the reflectivity terms ρ_{ab}, since they change continuously with polar angle. To solve this issue, averaged values of the reflectivities are calculated as

$$\bar{\rho}_{ab,ji} = \frac{\int_{\max(\theta_{b,j},\theta_{t,i})}^{\min(\theta_{b,j+1},\theta_{t,i+1})}\rho_{ab}(\theta_a)\cos(\theta_b)\sin(\theta_b)d\theta_b}{\int_{\max(\theta_{b,j},\theta_{t,i})}^{\min(\theta_{b,j+1},\theta_{t,i+1})}\cos(\theta_b)\sin(\theta_b)d\theta_b} \tag{18}$$

$$\bar{\rho}_{ab,j} = \frac{\int_{\theta_{b,j}}^{\theta_{b,j+1}}\rho_{ab}(\theta_a)\cos(\theta_b)\sin(\theta_b)d\theta_b}{\int_{\theta_{b,j}}^{\theta_{b,j+1}}\cos(\theta_b)\sin(\theta_b)d\theta_b}. \tag{19}$$

By substituting the averaged reflectivities into Eq. (17), the formula for the weighting parameter simplifies to

$$r_{ji} = \frac{1-\bar{\rho}_{ab,ji}}{1-\bar{\rho}_{ab,j}}\frac{\int_{\max(\theta_{b,j},\theta_{t,i})}^{\min(\theta_{b,j+1},\theta_{t,i+1})}\cos(\theta_b)\sin(\theta_b)d\theta_b}{\int_{\theta_{b,j}}^{\theta_{b,j+1}}\cos(\theta_b)\sin(\theta_b)d\theta_b} = \frac{1-\bar{\rho}_{ab,ji}}{1-\bar{\rho}_{ab,j}}\frac{D_{ji}}{D_j} \tag{20}$$

Fig. 4 gives a schematic representation of the heat flux calculation for each control angle of the medium b. The transmitted heat flux from each control angle of medium a, Eq. (15), is now obtained as $r_{ji}\dot{q}''_{a,i}$.

The weighting parameter r_{ji} in Fig. 4 indicate the fraction of the radiative heat flux within the control angle j in medium b which is initiated from the different control angles of the medium a. A matrix of weighting factors r_{ji} is obtained and the following matrix equation can be written for the radiative heat flux of different control angles:

$$\begin{bmatrix}\dot{q}''_{b,1}\\ \dot{q}''_{b,2}\\ .\\ .\\ .\\ \dot{q}''_{b,N}\end{bmatrix} = \begin{bmatrix}r_{11} & r_{12} & . & . & . & r_{1N}\\ r_{21} & r_{22} & . & . & . & r_{2N}\\ . & . & & & & .\\ . & . & & & & .\\ . & . & & & & .\\ r_{N1} & r_{N2} & . & . & . & r_{NN}\end{bmatrix}\begin{bmatrix}\dot{q}''_{a,1}\\ \dot{q}''_{a,2}\\ .\\ .\\ .\\ \dot{q}''_{a,N}\end{bmatrix} \tag{21}$$

Each row of the weighting factors matrix represents the shares of the different control angles of the first side in the heat flux of different control angles in the second side. By substituting the radiative heat fluxes Eqs. (13) and ((15)) into each row of the matrix Eq. (21), the following equation for each control angle of the second side of the interface is obtained:

$$\begin{aligned}&\int_{\Delta\psi}\int_{\theta_{b,j}}^{\theta_{b,j+1}} I_j\cos(\theta_b)\sin(\theta_b)d\theta_b d\psi\\ &=\sum_{i=1}^{N}\int_{\Delta\psi}\int_{\theta_{b,j}}^{\theta_{b,j+1}} r_{ji}I_i(1-\rho_{ab}(\theta_a))\left(\frac{n_b}{n_a}\right)^2\cos(\theta_b)\sin(\theta_b)d\theta_b d\psi\end{aligned} \tag{22}$$

Hence, the transmitted part of intensity is derived as:

$$I_{t,j} = \sum_{i=1}^{N} r_{ji}I_i(1-\bar{\rho}_{ab})\left(\frac{n_b}{n_a}\right)^2 \tag{23}$$

For the reflection part, the following equation is applied:

$$I_{r,j} = \bar{\rho}_{ba}I_j^- \tag{24}$$

where, I_j^- is the incoming radiation intensity to the interface. Therefore, by suming up the transmitted and reflected parts (Eqs. (23) and (24)), the following equation for the outgoing intensity from the interface is obtained as:

$$I_j^+ = \sum_{i=1}^{N} r_{ji}I_i(1-\bar{\rho}_{ab,i})\left(\frac{n_b}{n_a}\right)^2 + \bar{\rho}_{ba}I_j^- \tag{25}$$

2.2.1. Efficiency considerations

For two media with the same refractive indexes, the weighting parameter matrix will be an identity matrix. For modeling radiation from a medium with a lower refractive index to a medium with a higher refractive index, the weighting parameter matrix is an upper triangular matrix and for modeling radiation in the reverse direction, the weighting matrix is a lower triangular matrix. In any case, most of the elements of the weighting matrix are zeros. Therefore, we can skip calculating parts of the weighting matrix to speed up the calculations. Moreover, the intensity within the medium with higher refractive index is fully reflected for the control angles higher than the critical angle. For these control angles, the calculation of weighting parameters should be skipped because there is not any transmission to or from the adjacent medium. Finally each control angle can only receive transmitted intensity from a few control angles of the adjacent medium depending on the used angular discretization. For example, for $n_a > n_b$, the first control angle in medium a receives intensity from the first control angle of the medium b only and the other control angles can only receive the intensity from the limited number of control angles of medium b.

2.3. Diffuse boundary

The diffuse boundary condition is commonly applied for modeling the thermal radiation transfer at the interface of two different

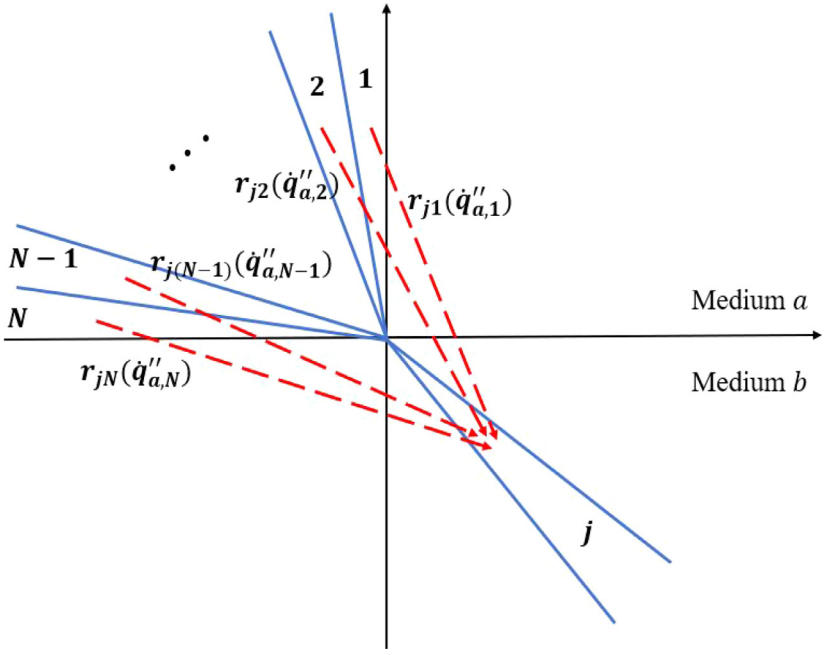

Fig. 4. The transmitted heat flux from different control angles in medium a which may end up a control angle of medium b.

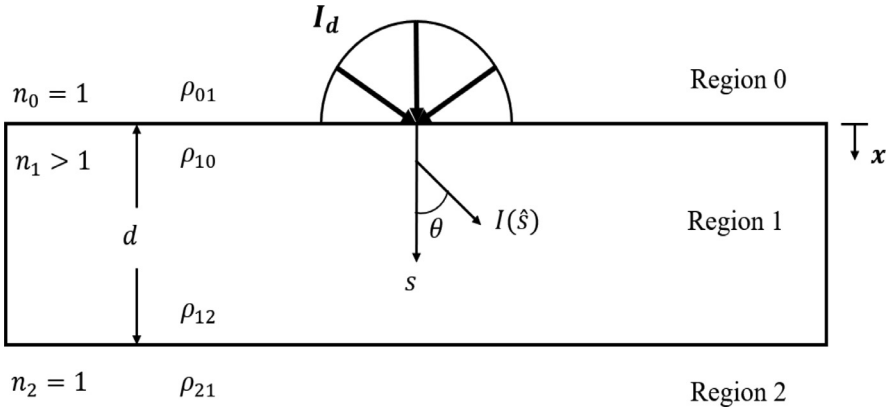

Fig. 5. The considered geometry of the first case study.

materials. This assumption does not consider the angular distribution at the boundaries and divides the radiative energy equally between the different control angles. Hence, the boundary condition at the second side of the interface is given by

$$I^+ = (1-\bar{\rho}_{01})I_d + \frac{\bar{\rho}_{10}}{\pi}\int_{\hat{n}.\hat{s}<0} I^-|\hat{n}.\hat{s}|d\Omega \tag{26}$$

It is applied in one of our test cases to address the effect of this assumption on the radiative heat source distribution. Without applying the Fresnel relation, the determined reflectivity for a diffuse boundary is just an estimation. In this paper, to enhance the accuracy of modeling with the diffuse boundary assumption, the average reflectivities used in Eq. (26) are calculated by Eq. (19).

3. Test cases and benchmark solutions

3.1. One-layer slab with diffuse irradiation at the upper boundary

The first case study is a one-layer slab with a thickness of d and a refractive index of n_1 that is surrounded by two regions with a refractive index of unity as has been shown in Fig. 5. The absorption and scattering coefficients of the layer are assumed to be constants, and a diffuse intensity enters the layer from its upper region. To solve the radiation transfer within the layer, two boundary conditions for the upper and bottom interfaces are introduced. The boundary condition for the upper interface is:

$$I^+(0,\mu_1) = (1-\rho_{01}(\mu_0))\left(\frac{n_1}{n_0}\right)^2 I_d + \rho_{10}(\mu_1)I^-(0,-\mu_1) \tag{27}$$

where ρ_{ij} shows the reflectivity at the interface where the radiation propagates from medium i to medium j. For the bottom interface, the boundary condition is:

$$I^-(d,-\mu_1) = \rho_{12}(\mu_1)I^+(d,\mu_1) \tag{28}$$

An analytical solution for the forward and backward intensities is given in Appendix B. Using these intensities, the radiative heat flux and irradiation are given as:

$$\begin{aligned}\dot{q}''(x) &= 2\pi\int_{-1}^{1} I(x,\mu)\mu d\mu \\ &= 2\pi\left(\int_0^1 I^+(x,\mu)\mu d\mu - \int_0^1 I^-(x,\mu)\mu d\mu\right)\end{aligned} \tag{29}$$

$$G(x) = 2\pi\int_{-1}^{1} I(x,\mu)d\mu = 2\pi\left(\int_0^1 I^+(x,\mu)d\mu + \int_0^1 I^-(x,\mu)d\mu\right) \tag{30}$$

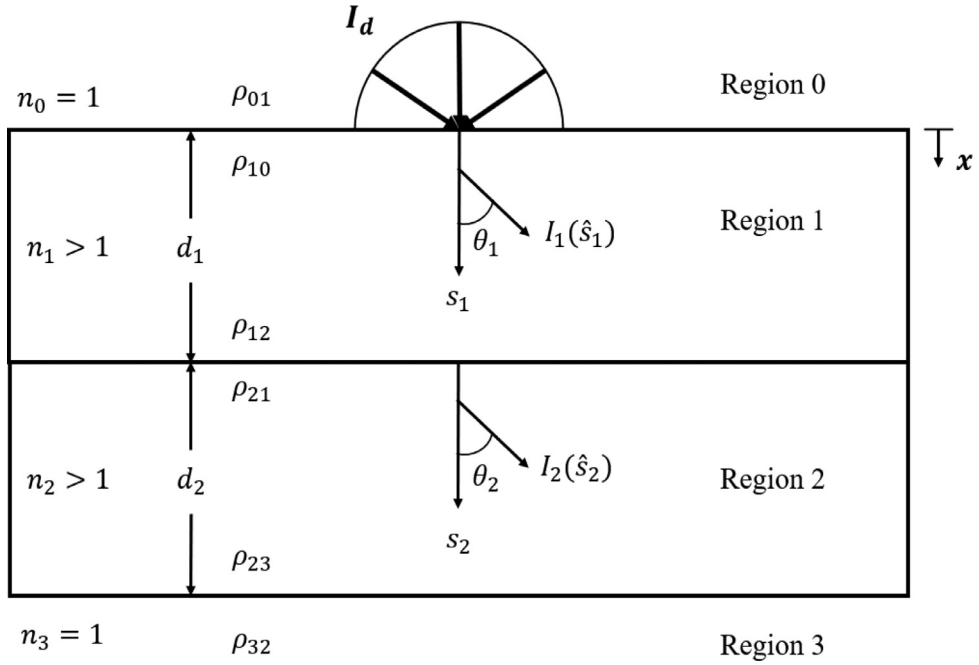

Fig. 6. The considered geometry of the second case study.

The reflectivity from the interface of regions 0 and 1 is:

$$R = \frac{2}{I_d}\left(\int_0^1 [1-\rho_{10}(\mu_1)]I^-(0,\mu_1)\mu_1 d\mu_1 + I_d\int_0^1 \rho_{01}(\mu_0)\mu_0 d\mu_0\right) \tag{31}$$

and the transmissivity from the bottom surface of region 1 is:

$$T = \frac{2}{I_d}\int_0^1 [1-\rho_{12}(\mu_1)]I^+(d,\mu_1)\mu_1 d\mu_1 \tag{32}$$

In the Appendix B, the analytical solutions are given for the different forms of phase function including: zero phase function (pure absorption), isotropic phase function, linear, and nonlinear anisotropic phase functions.

3.2. Two-layer slab with diffuse irradiation at the upper boundary

For the second case study, as has been shown in Fig. 6, a two-layer slab with the refractive indexes of n_1 and n_2 and the thicknesses of d_1 and d_2 for the first and second layers are considered. These two layers are surrounded by two regions with a refractive index of unity and a diffusive intensity enters from the region 0 to the region 1 (i.e. first layer). To solve the radiation transfer within the two layers, four boundary conditions are needed. The boundary condition for the upper interface of region 1 is:

$$I_1^+(0,\mu_1) = (1-\rho_{01}(\mu_0))\left(\frac{n_1}{n_0}\right)^2 I_d + \rho_{10}(\mu_1)I_1^-(0,-\mu_1) \tag{33}$$

For the interface of region 1 and region 2, the boundary condition for the side facing region 1 is:

$$I_1^-(d_1,-\mu_1) = (1-\rho_{21}(\mu_2))\left(\frac{n_1}{n_2}\right)^2 I_2^-(0,-\mu_2) + \rho_{12}(\mu_1)I_1^+(d_1,\mu_1) \tag{34}$$

For the upper interface of the region 2, the boundary condition is described by the following equation:

$$I_2^+(0,\mu_2) = (1-\rho_{12}(\mu_1))\left(\frac{n_2}{n_1}\right)^2 I_1^+(d_1,\mu_1) + \rho_{21}(\mu_2)I_2^-(0,-\mu_2) \tag{35}$$

The last boundary condition is for the bottom surface of region 2:

$$I_2^-(d_2,-\mu_2) = \rho_{23}(\mu_2)I_2^+(d_2,\mu_2) \tag{36}$$

For different forms of the phase function, the analytical solutions for the second test case are given in Appendix C.

4. Results and discussion

4.1. Mesh independence study

The mesh independence of the numerical solutions has been investigated by monitoring radiative heat flux, and irradiation obtained by using different grid sizes. For the first and second case studies in the pure absorption state, Fig. 7 shows the variation of the normalized heat flux and normalized irradiation within the medium for three different grid sizes. Most of the results are presented with respect to the optical thickness (τ) that is defined as $\tau = \beta \times x$. The difference between the results of using the grid with the optical thicknesses of 0.01 and 0.005 in the one-layer slab and of using the grid sizes of 1 cm and 5 mm in the two-layer slab were less than 1%. Therefore, using the grid with optical thickness of 0.01 in the first case study and 1 cm in second case study assure mesh independence of the results.

4.2. Results for the first case study

Having reflection or scattering makes the radiation solution iterative, therefore a convergence criterion is needed. For the first and second case studies, the following convergence condition for irradiation (G) is applied [39]:

$$\max\left|\frac{G_p^N - G_p^{N-1}}{G_p^N}\right| \le 10^{-4} \tag{37}$$

where the superscripts N and $N-1$ represent the current and previous steps, respectively.

To investigate the accuracy of the OWM for the Fresnel interface, results of the normalized radiative heat flux, normalized irradiation, reflectivity, transmissivity, and directional intensity will

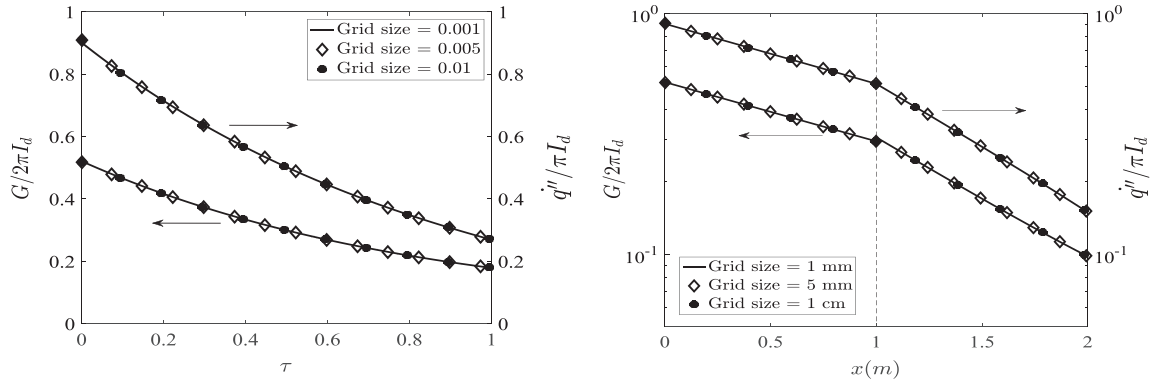

Fig. 7. Mesh independence study for the normalized heat flux and normalized irradiation in: left) one-layer slab with $\beta_1 = 1$, $n_1 = 1.5$ and right) two-layer slab with $\kappa_1 = 0.5$, $\kappa_2 = 1$, $n_1 = 1.5$, and $n_2 = 1.333$.

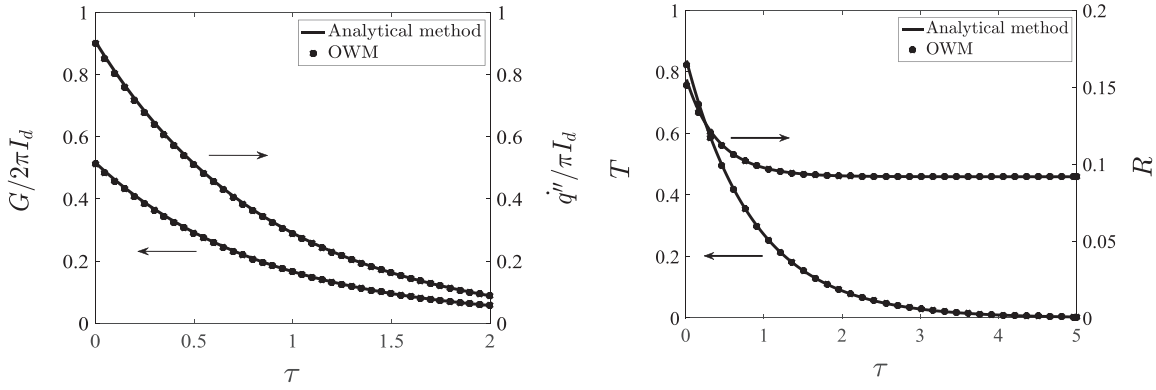

Fig. 8. The normalized radiative heat flux with normalized irradiation (left) and reflectivity with transmissivity (right) for one-layer slab with $\beta_1 = 1$, $n_1 = 1.5$.

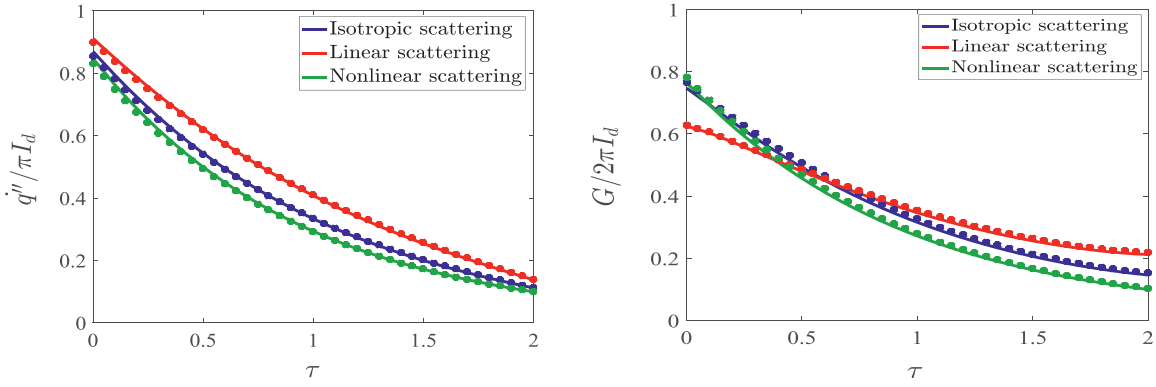

Fig. 9. The normalized radiative heat flux (left) and normalized irradiation (right) for different types of scattering in one-layer slab with $\beta_1 = 1$, $\sigma_{s,1} = 0.5$, and $n_1 = 1.5$; solid line: analytical results, and marker: numerical results.

be compared to the analytical results. For all the presented results, the polar and azimuthal angles within the sphere octant have been discretized into 32 segments. Fig. 8 shows the results for both analytical and OWM within the one-layer slab with respect to the optical thickness. For the transmissivity and reflectivity, the results have been presented with respect to the total optical thickness of the layer. These results were obtained for the pure absorption case. Diagrams in Fig. 8 show an excellent agreement between the analytical and numerical results. For the scattering media, different types of phase functions have been applied within the calculations. All the analytical solutions for scattering media in this paper have been extracted using the Nyström method [40] with 48 quadrature points. For the linear scattering, the assumption of $a = 1.843041$ was used (see Eqs. (4) and (5)). The normalized heat flux and normalized irradiation for three types of phase functions have been presented in Fig. 9. It is worth reminding that the nonlinear scattering in the present work is based on Eq. (6). For the scattering media, the accuracy is lower compared to the pure absorption case that suggests applying finer angular discretizations. For the reflectivity and transmissivity from the upper and bottom interfaces of the one-layer slab, Fig. 10 shows the results of the analytical and the OWM for three different optical thicknesses with respect to the refractive index of the medium. These results are for scattering media with isotropic scattering phase function. According to Fig. 10, for higher optical thicknesses, the results of the numerical method are in excellent agreement with the analytical results. However, for the lower optical thicknesses, the averaged error is around 1%. To show the simulation results in more details, the variation of radiation intensity in the forward direction has been presented at different depths of the medium in Fig. 11. Note

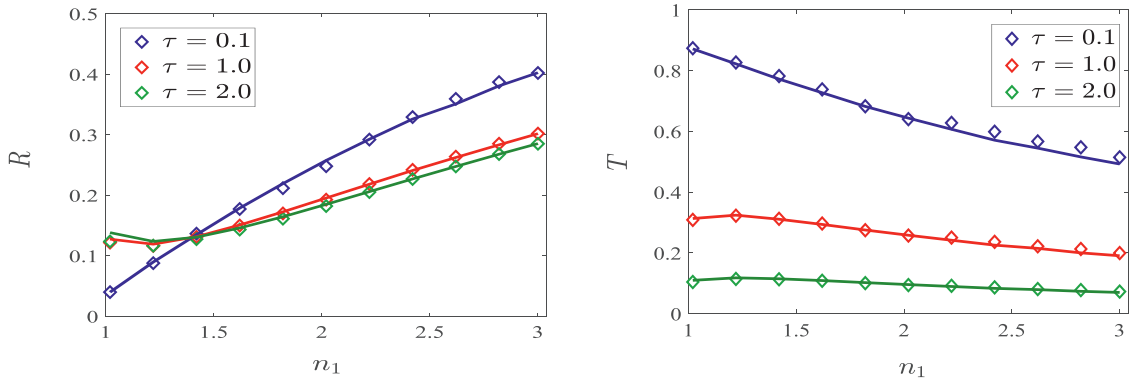

Fig. 10. The reflectivity (left) and transmissivity (right) for different optical thicknesses in one-layer slab with $\beta_1 = 1$; solid line: numerical results, and marker: analytical results.

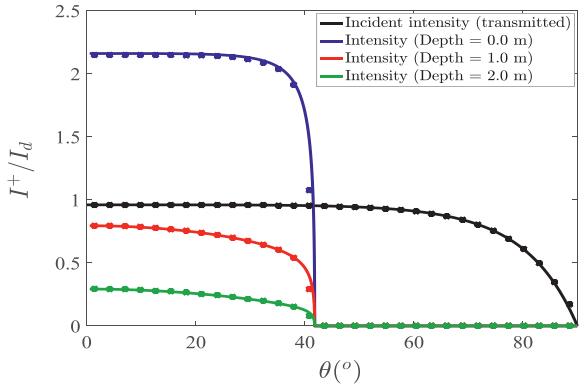

Fig. 11. The directional intensities at different depths of the one-layer slab in pure absorption state with $\beta_1 = 1$, $n_1 = 1.5$; solid line: analytical results, and marker: numerical results.

that the incident transmissivity defined as the ratio of the forward intensity to the diffuse intensity at the boundary (I^+/I_d) does not begin with unity which is due to reflection from the surface. By passing through the interface, the magnitude and direction of the intensity are changed due to the different refractive indexes of the two adjacent media. Therefore, the transmitted intensity converts to the intensity at depth 0 (i.e. blue line) that is the intensity at the other side of the interface facing the second medium. As the media of the first test case were non-scattering, the direction of the intensity will remain unchanged but its magnitude decreases due to the medium absorption. To show the accuracy of the OWM, the intensities of different directions calculated by the numerical and analytical methods have been compared in Fig. 11. The results show good accuracy for the simulated directional intensities. To study the effect of assuming diffuse radiation for modeling Fresnel interface, the predicted radiative heat source and heat flux for the one-layer slab are given in Fig. 12. For Fresnel interface, the irradiation is less absorbed due to the smaller solid angle at the optically dense side. Therefore, the radiative heat source is lower and heat flux is higher for this type of interface compared to the diffuse interface.

4.3. Results for the second case study

For the second case study, the normalized heat flux, normalized irradiation, transmissivity at the bottom surface of region 2, and reflectivity of the upper surface of region 1 have been presented for both analytical and OWM for the case of pure absorption. Similar to the first case study, transmissivity and reflectivity have been plotted with respect to the optical length of the medium. An excellent agreement between the analytical and numerical results proves the high accuracy of the presented method for the pure absorption case. In Fig. 14 different absorption coefficient have been assumed for each of the two non-scattering layers where the normalized radiative heat flux and normalized irradiation have been plotted in semi-logarithmic scale. With semi-logarithmic scale, the results are shown as straight lines which is due to media's absorption exponential decay. The interface of the two layers has been shown with a dashed line. For the scattering media, similar to the first-layer case study, three different phase functions have been considered. The normalized radiative heat flux and normalized irradiation have been shown in Fig. 15. As explained in the model description section, only the radiative heat flux is conserved at the interface of the two media. The presented results show this fact at

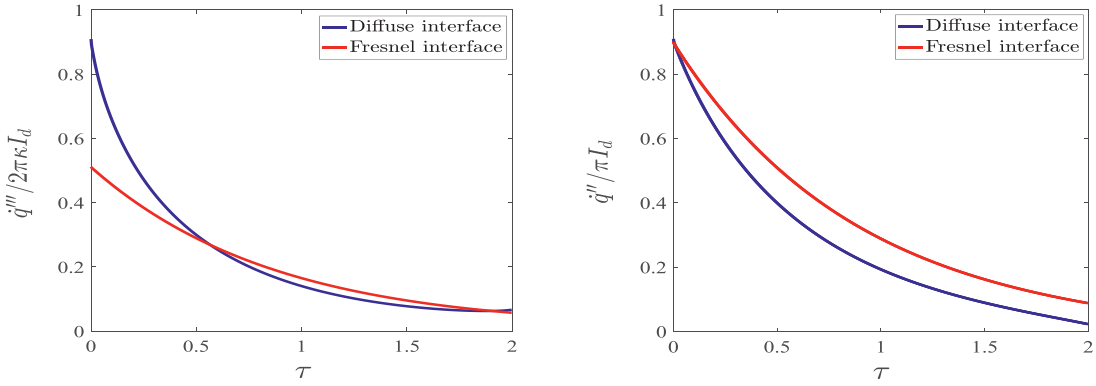

Fig. 12. The normalized radiative heat source (left) and normalized radiative heat flux (right) for diffuse and Fresnel interface in one-layer slab of absorbing and non-scattering medium with $\beta_1 = 1$, $n_1 = 1.5$.

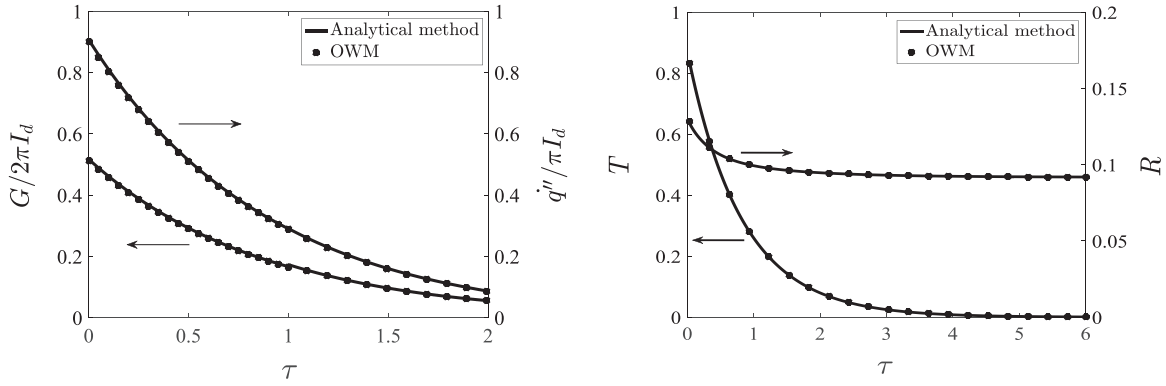

Fig. 13. The normalized radiative heat flux with normalized irradiation (left) and reflectivity with transmissivity (right) for two-layer slab in pure absorption state with $\beta_1 = 0.5$, $\beta_2 = 1$, $n_1 = 1.5$, and $n_2 = 1.333$.

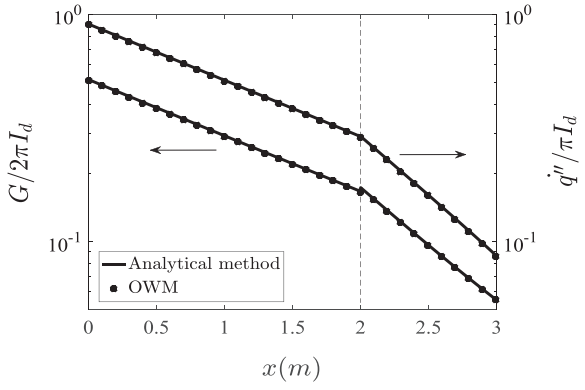

Fig. 14. The normalized radiative heat flux and normalized irradiation for two-layer slab in pure absorption state with $\beta_1 = 0.5$, $\beta_2 = 1$, $n_1 = 1.5$, and $n_2 = 1.333$.

the interface that is located at the optical thickness of 1. Unlike the normalized heat flux, the normalized irradiation is not conserved and a step is observed in normalized irradiation profiles at the interface. This is not only due to the reflection at the interface, but also due to the change in the solid angle of the intensities that is occurred for media with different refractive indexes. To study the capability of the OWM in estimating the reflectivity and transmissivity of a scattering media, the analytical solution presented for the isotropic scattering media in [41] have been used as the benchmark solution here. The results are presented for three different optical thicknesses in Fig. 16. Similar to the one-layer case study, the accuracy of the simulation increases with increment of the optical thickness. Finally, the angular distribution of the intensity in the forward direction has been plotted in Fig. 17 at the location of interfaces. As explained for the one-layer case, the magnitude and angular distribution of the intensity change while passing the interface. By going from a medium with a lower refractive index to the medium with a higher refractive index, the magnitude of the intensity increases but its solid angle span is reduced and vice versa. A comparison has been done between the analytical and numerical results for the directional intensities. The presented results confirm the good accuracy of the OWM for estimation of the directional intensities of the two-layer slab, too.

Table 1
The averaged relative errors of the OWM for different case studies.

Medium	One-layer		Two-layer	
	$\delta\dot{q}''$ (%)	δG (%)	$\delta\dot{q}''$ (%)	δG (%)
Pure absorption	0.07	0.27	0.90	0.85
Isotropic scattering	0.88	3.2	2.9	4.5
Linear scattering	0.92	2.1	1.9	1.9
Nonlinear scattering	0.81	2.7	2.6	4.9

To summarize the accuracy of the OWM for different case studies, Table 1 includes the quantitative values for the averaged relative error of radiative heat flux and irradiation. The given averaged relative errors in Table 1 are calculated as

$$\delta\Phi = \frac{1}{m}\sum_{i=1}^{m}\frac{|\Phi_{an}-\Phi_{num}|}{\Phi_{an}}\times 100\% \tag{38}$$

where Φ_{an} and Φ_{num} are the analytically and numerically calculated values of Φ, respectively, and Φ is either $\dot{q}''$ or G.

To show the applicability of the OWM for different types of angular discretization, a new non-uniform angular dicretization has also been investigated that produces relatively equal solid angles

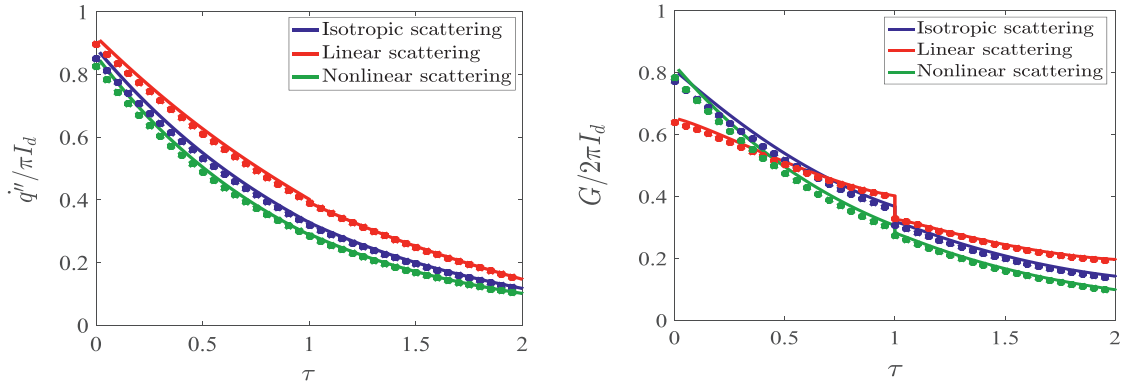

Fig. 15. The normalized radiative heat flux (left) and normalized irradiation (right) by applying different types of scattering phase function for two-layer slab with $\sigma_{s,1}/\beta_1 = 0.5$, $\sigma_{s,2}/\beta_2 = 0.5$, $n_1 = 1.5$, and $n_2 = 1.333$; solid line: analytical results, and marker: numerical results.

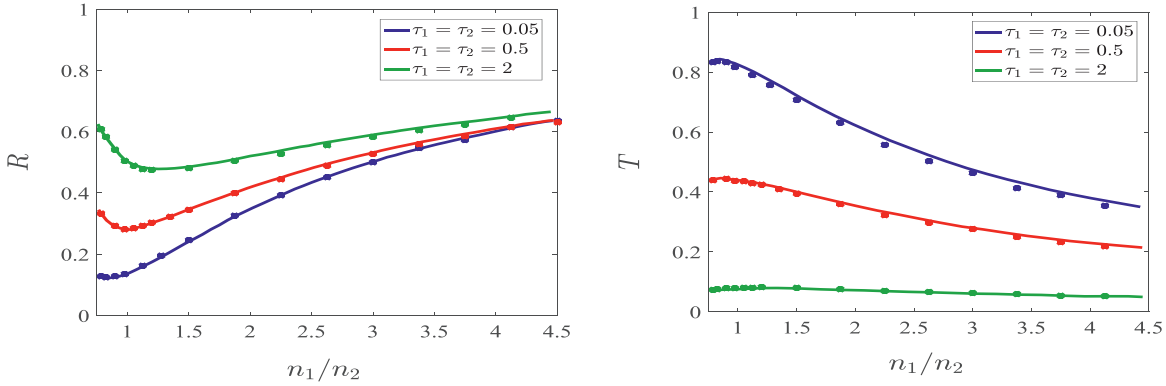

Fig. 16. The reflectivity (left) and transmissivity (right) in two-layer slab with $\sigma_{s,1}/\beta_1 = 1$, $\sigma_{s,2}/\beta_2 = 0.7$, $n_1 = 1.5$, and $n_2 = 1.333$; solid line: analytical results [41], and marker: numerical results.

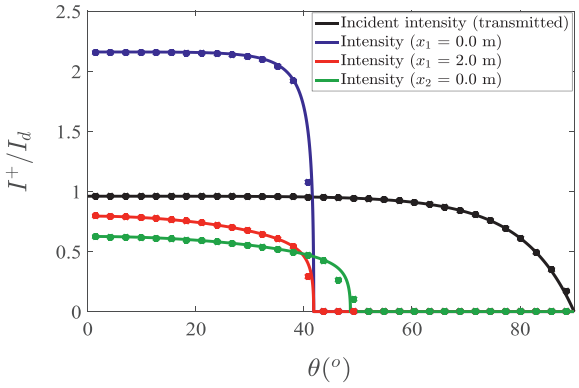

Fig. 17. The directional intensities at the location of interfaces in pure absorption case of two-layer slab with $\beta_1 = 0.5$, $\beta_2 = 1$, $n_1 = 1.5$, and $n_1 = 1.333$; solid line: analytical results, and marker: numerical results.

Table 2
The effect of the angular resolution on the difference between simulated and benchmark results for transmissivity of the two-layer slab with: $\sigma_{s,1}/\beta_1 = 1.0$, $\sigma_{s,2}/\beta_2 = 0.0$, $n_1 = 1.5$, $n_2 = 1.333$, $\tau_1 = 1.0$, and $\tau_2 = 0.5$.

Angular discretization	Benchmark solutions	OWM	Error (%)
2 × 2	0.26519	0.22524	15.06
4 × 4	0.26519	0.23655	10.80
8 × 8	0.26519	0.25197	4.99
12 × 12	0.26519	0.25893	2.36
16 × 16	0.26519	0.26202	1.20
24 × 24	0.26519	0.26523	0.02

in different directions. The detailed formulation of this discretization scheme has been given in [42]. A comparison of the results obtained using uniform and non-uniform solid angle discretization schemes with the same number of control angles is presented in Fig. 18 for the normalized irradiation and heat flux. The results are shown for the one- and two-layer slabs with the same conditions as those of Figs. 8 and 13. The results obtained using the two discretization schemes are practically identical, which confirms the applicability of the OWM with different types of discretizations.

While all the results so far were obtained for 32×32 control angles of the sphere octant, the results of the OWM for the coarser solid angle discretizations are compared with the analytical results of [41] in Table 2 for transmissivity and Table 3 for reflectivity into region 0. The transmissivities (Table 2) show that by coarsening the angular discretization to 8×8, the error is still lower than 5%. For the reflectivity into region 0, the reported results in Table 3 show an excellent accuracy even for the coarsest angular discretization of 2×2. It appears that the accuracy of the predicted reflectivity remains better than that of transmissivity at the coarse angular resolutions.

Table 3
The effect of the angular resolution on the difference between simulated and benchmark results for reflectivity of the two-layer slab with: $\sigma_{s,1}/\beta_1 = 1.0$, $\sigma_{s,2}/\beta_2 = 0.0$, $n_1 = 1.5$, $n_2 = 1.333$, $\tau_1 = 1.0$, and $\tau_2 = 0.5$.

Angular discretization	Benchmark solutions	OWM	Error (%)
2 × 2	0.30520	0.30206	1.03
4 × 4	0.30520	0.30144	1.23
8 × 8	0.30520	0.30322	0.65
12 × 12	0.30520	0.30333	0.61
16 × 16	0.30520	0.30374	0.48
24 × 24	0.30520	0.30479	0.13

To compare the accuracy of the OWM against the Murthy's pixelation method, both methods were used for calculating transmissivity through the two-layer slab. The results are shown in Table 4 for three different angular resolutions and two different pixelation resolutions for each of the angular resolutions. The results show that by applying the same number of control angles in both methods and a single pixel, OWM is more accurate than the pixelation method at all resolutions. Adding 10×10 pixels for each control angle makes the pixelation method more accurate at low angular resolutions.

Implementing the Murthy's pixelation method requires the computation of several variables, such as the reflectivity and radiative heat flux, for each pixel. In addition, the angles at both sides of the interface need to be determined, and the corresponding control angle identified. To assure good accuracy, these parameters must be calculated at each time step. The benefit of the present OWM is that the weighting matrix is calculated only once in the beginning of the simulations, and the summation in Eq. (25) is done for less than half of the matrix elements by efficient programming. Lower CPU time is thus expected for the OWM. To quantify the computational costs, simulations were performed for the one-layer medium (i.e. first case study) in pure absorption state with $\beta_1 = 1$ and $n_1 = 1.5$ using 400 grids. Table 5 gives the averaged relative errors of the radiative heat flux and irradiation of the two methods together with their CPU times. The calculations were done using MATLAB codes with similar programming logic on the same computer (Intel core i7 6500U processor). As seen in Table 5, the Murthy's pixelation method requires 6 to 19 times more CPU time than the OWM. For the finest solid angle discretization, which is more commonly used in CFD models, the accuracy of OWM is better than the Murthy's pixelation method. Nonetheless, the Murthy's pixelation method provides slightly more accurate results at coarse angular resolutions, yet with the cost of longer computational time.

Finally, the performance of the OWM is studied at different absorption and scattering states of the two-layer slab. The prediction errors of the transmissivity and reflectivity are given in Table 6 for six different radiative property combinations. The simulation

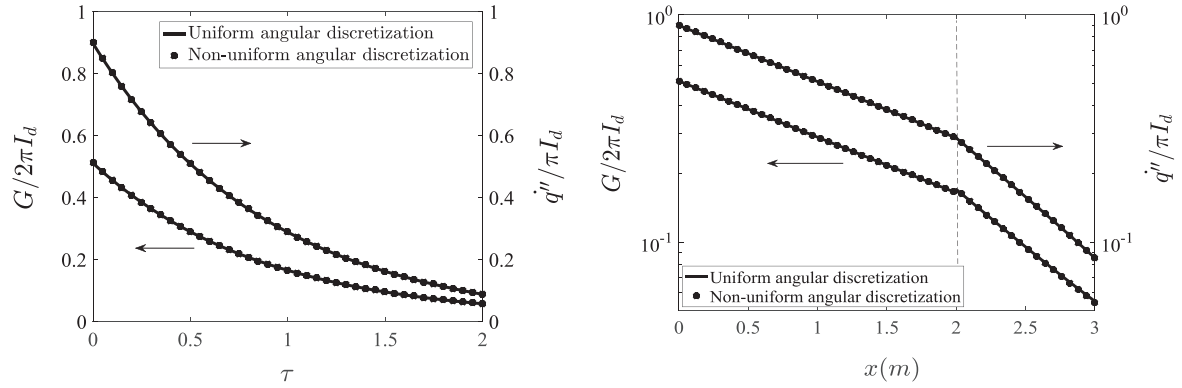

Fig. 18. The normalized radiative irradiation and heat flux for one-layer (left) and two-layer (right) slabs with uniform and nonuniform angular discretizations.

Table 4
Comparison of the OWM and the Murthy's pixelation method predictions for transmissivity of the two-layer slab with: $\sigma_{s,1}/\beta_1 = 1.0$, $\sigma_{s,2}/\beta_2 = 0.0$, $n_1 = 1.5$, $n_2 = 1.333$, $\tau_1 = 1.0$, and $\tau_2 = 0.5$.

Angular	OWM		Angular discretization	Murthy's Pixelation method	
discretization	Transmissivity	Error (%)	together with pixels	Transmissivity	Error (%)
2×2	0.22524	15.06	2×2 × 1×1	0.322	21.42
			2×2 × 10×10	0.238	10.25
4×4	0.23655	10.80	4×4 × 1×1	0.308	16.14
			4×4 × 10×10	0.254	4.22
8×8	0.25197	4.99	8×8 × 1×1	0.245	7.61
			8×8 × 10×10	0.266	0.31

Table 5
Comparison of the accuracy of OWM with the Murthy's pixelation method for a one-layer slab with $\beta_1 = 1$ and $n_1 = 1.5$.

Angular	OWM			Angular discretization	Murthy's pixelation method		
discretization	$\delta\dot{q}''$ (%)	δG (%)	CPU time (s)	together with pixels	$\delta\dot{q}''$ (%)	δG (%)	CPU time (s)
4×4	7.6	1.9	0.003	4×4 × 10×10	3.7	1.8	0.019
8×8	3.4	1.3	0.008	8×8 × 10×10	1.9	1.2	0.058
16×16	0.24	0.48	0.015	16×16 × 10×10	0.52	0.54	0.280

Table 6
The simulation error of the transmissivity and reflectivity for different states of the two-layer media.

$\sigma_{s,1}/\beta_1$	$\sigma_{s,2}/\beta_2$	τ_1	τ_2	n_1	n_2	Error of transmissivity (%)	Error of reflectivity (%)
0.2	0.8	1.0	0.5	1.5	1.333	0.03	0.15
0.8	0.2	0.5	1.0	1.333	1.5	0.69	0.78
1.0	0.0	1.0	0.5	1.5	1.333	0.02	0.13
0.0	1.0	0.5	1.0	1.333	1.5	0.75	0.26
1.0	1.0	1.0	0.5	1.5	1.333	1.17	1.05
1.0	1.0	0.5	1.0	1.333	1.5	1.93	2.27

results were obtained with 24×24 angular discretization for the sphere octant. The results prove the good accuracy of the OWM for a wide range of states. For the pure scattering cases, however, the error increases compared to the other states, suggesting a need for higher number of discretiztaion angles.

5. Conclusions

At the interface of optically different materials known as the Fresnel interface, the magnitude and direction of the radiation intensity change which in turn alters the irradiation. A new numerical method for considering the Fresnel interface in the FVM has been presented in this paper. The novel ordinate weighting method (OWM) is based on the conservation of radiative heat flux at the interface and provides the angular intensity distribution on the other side of the interface with high accuracy and low computational cost. For the numerical implementation, the weighting parameters are calculated for the each pair of control angles at the two sides of the interface. The weighting parameters represent the share of the radiative heat flux within a control angle on the second side of the interface that originates from a specific control angle on the first side.

To investigate the accuracy of the OWM, benchmark solutions were developed for one- and two-layer case studies with different properties by applying the Nyström method with high number of quadrature points. For the scattering media, different types of scattering phase function were considered, including isotropic, linear and nonlinear scattering phase functions. The OWM predictions for several radiation parameters, such as the normalized irradiation and radiative heat flux, reflectivity from the upper surface, transmissivity from the bottom surface, and the directional intensity, were in excellent agreement with the analytical solutions and the previously reported data of the literature. Comparing the OWM predictions against the Murthy's pixelation method showed that the OWM exhibits better performance both in terms of accuracy and computational time. To show the applicability of the OWM with different types of angular discretizations, simulations were carried out for non-uniform and uniform angular discretizations

with the same number of control angles. The results for the two discretization schemes were practically identical, proving the capability of the OWM in supporting different solid angle discretization schemes. Finally, the accuracy over a range of different radiative properties was demonsrated.

In this paper, the OWM was presented for a flat interface in one-dimensional geometry, discretized with a structured mesh. Implementing this method to the cases with unstructured mesh and non-flat interface are some of the potential ideas for continuation of the research.

Declaration of Competing Interest

Reffering to manuscript entitled as "The ordinate weighting method for solving radiative heat transfer through a Fresnel interface" published in Journal of Quantitative Spectroscopy and Radiative Transfer. We wish to confirm that there are no known conflicts of interest associated with this publication and there has been no significant financial support for this work that could have influenced its outcome. We confirm that the manuscript has been read and approved by all named authors and that there are no other persons who satisfied the criteria for authorship but are not listed. We further confirm that the order of authors listed in the manuscript has been approved by all of us. We confirm that we have given due consideration to the protection of intellectual property associated with this work and that there are no impediments to publication, including the timing of publication, with respect to intellectual property. In so doing we confirm that we have followed the regulations of our institutions concerning intellectual property. We understand that the Corresponding Author is the sole contact for the Editorial process (including Editorial Manager and direct communications with the office). He is responsible for communicating with the other authors about progress, submissions of revisions and final approval of proofs. We confirm that we have provided a current, correct email address which is accessible by the Corresponding Author.

CRediT authorship contribution statement

Farid Alinejad: Conceptualization, Methodology, Software, Validation, Formal analysis, Investigation, Resources, Data curation, Writing- Original draft preparation, Visualization. **Hadi Bordbar:** Conceptualization, Methodology, Resources, Writing - Review & Editing, Investigation, Supervision, Project administration. **Simo Hostikka:** Conceptualization, Methodology, Writing - Review & Editing, Supervision, Project administration, Funding acquisition.

Acknowledgment

The authors greatly acknowledge the support of the Academy of Finland under grant no. 314487 and the Finnish Fire Protection Fund (Palosuojelurahasto).

Appendix A

For the transmitted part of the incident intensity with solid angle of $\Delta\Omega_a$, the radiative heat flux is calculated using the following equation:

$$\dot{q}''_a = \int_{\Delta\psi}\int_{\Delta\theta_a} I(1-\rho_{ab}(\theta_a))\cos\theta_a \sin\theta_a d\theta_a d\psi \tag{A.1}$$

Passing a Fresnel interface, the direction of intensity changes. Therefore, the direction of θ_a for the intensity in medium a changes to θ_b in medium b. The relation of these two angles is given by Snell's law. Therefore, the radiative heat flux at other side of the interface is calculated using the equation:

$$\dot{q}''_b = \int_{\Delta\psi}\int_{\Delta\theta_b} I(1-\rho_{ab}(\theta_a))\left(\frac{n_b}{n_a}\right)^2 \cos\theta_b \sin\theta_b d\theta_b d\psi \tag{A.2}$$

Differentiating the equation of Snell's law gives:

$$n_a cos\theta_a d\theta_a = n_b cos\theta_b d\theta_b \tag{A.3}$$

Therefore, applying the Eqs. (A.2) and (A.3) gives the following relation for θ_a and θ_b:

$$cos\theta_b sin\theta_b d\theta_b = \left(\frac{n_a}{n_b}\right)^2 cos\theta_a sin\theta_a d\theta_a \tag{A.4}$$

Replacing the above equation into Eq. (A.2), gives the equality of $\dot{q}''_a$ and $\dot{q}''_b$.

Appendix B

The solution of radiation transfer in a one-layer slab with diffuse irradiation at the boundary for the forward radiation intensity is given as:

$$I^+(x,\mu_1) = (A(\mu)+\rho_{10}B(\mu))exp\left(-\beta\frac{x}{\mu_1}\right) + \rho_{10}\int_0^d exp\left(-\beta\frac{x+x'}{\mu_1}\right)S(x',-\mu_1)\frac{dx'}{\mu_1} + C(0,x,\mu) \tag{B.1}$$

For the backward radiation, the analytical solution for the intensity is given as:

$$I^-(x,-\mu_1) = C(x,d,\mu) + B(\mu)exp\left(\frac{\beta x}{\mu_1}\right) \tag{B.2}$$

In the above equations, A, B, and C are defined as:

$$A(\mu) = \left(\frac{n_1}{n_0}\right)^2(1-\rho_{01}(\mu_0))I_d \tag{B.3}$$

$$B(\mu) = \rho_{12}\frac{C(0,d,\mu)+\rho_{10}\int_0^d \exp\left(-\frac{\beta x'}{\mu_1}\right)S(x',-\mu_1)\frac{dx'}{\mu_1} + \int_0^d \exp\left(\frac{\beta x'}{\mu_1}\right)S(x',\mu_1)\frac{dx'}{\mu_1}}{\exp\left(\frac{2\beta d}{\mu_1}\right)-\rho_{10}\rho_{12}} \tag{B.4}$$

$$C(a,b,\mu) = \int_a^b exp\left(\beta\frac{x-x'}{\mu_1}\right)S(x',-\mu)\frac{dx'}{\mu_1} \tag{B.5}$$

where, the source term is defined by:

$$S(x',\mu) = \frac{\sigma_s}{4\pi}\int_{4\pi} I(x',\mu')\phi(\mu_0)d\Omega \tag{B.6}$$

Appendix C

For the two layer media with diffuse irradiation at the upper boundary, the analytical solution for the forward radiation intensity within region 1 is given as:

$$I_1^+(x_1,\mu_1) = \left(A + \frac{G\left(\rho_{23}\left((1-\rho_{12})E_1(2d_1)E_2(2d_2)\left(An_{12}^2+D_{12}(0,d_1)\right)+E_2(2d_2)D_{22}(0,d_2)\right)\right)}{J} + \frac{GD_{21}(0,d_2)+\rho_{10}H\left(\rho_{12}An_{20}^2E_1(2d_1)+D_{11}(0,d_1)(1+\rho_{12}E_1(2d_1))\right)}{J}\right)E_1(d_1)+E_1(x_1)D_{12}(0,x_1) \tag{C.1}$$

For the backward intensity within the region 1, the analytical solution is:

$$I_1^-(x_1,-\mu_1) = BI_1^+(d_1,\mu_1) + (1-\rho_{21})n_{12}^2(D_{21}(0,d_2)+F)E_1(d_1-x_1) + E_1(-x_1)D_{11}(x_1,d_1) \tag{C.2}$$

For the region 2, the analytical solution of the forward radiation intensity is given as:

$$I_2^+(x_2,\mu_2) = (n_{21}^2((1-\rho_{12})+\rho_{21}B)I_1^+(d_1,\mu_1) + \rho_{21}(D_{21}(0,d_2)+F)+D_{22}(0,x_2))E_2(x_2) \quad (C.3)$$

Finally, for the backward radiation intensity within the region 2, the analytical solution is:

$$I_2^-(x_2,-\mu_2) = n_{21}^2 B I_1^+(d_1,\mu_1)E_2(d_2-x_2)+(F+D_{21}(x_2,d_2))E_2(-x_2) \quad (C.4)$$

where the included parametres are defined as follows:

$$A = (1-\rho_{01})\left(\frac{n_1}{n_0}\right)^2 I_d \quad (C.5)$$

$$B = \frac{\rho_{23}(1-\rho_{12})E_2(d_2)}{H} \quad (C.6)$$

$$C = \rho_{12}+(1-\rho_{21})B \quad (C.7)$$

$$D_{ij}(a,b) = \int_a^b E_i((-1)^{j+1}x_i')S(x_i',(-1)^j\mu_i)\frac{dx_i'}{\mu_i} \quad (C.8)$$

$$E_i(x_i) = exp\left(-\frac{\beta_i x_i}{\mu_i}\right) \quad (C.9)$$

$$F = \rho_{23}\frac{\rho_{21}D_{21}(0,d_2)+D_{22}(0,d_2)}{1-\rho_{21}\rho_{23}E_2(2d_2)}E_2(d_2) \quad (C.10)$$

$$G = \rho_{10}(1-\rho_{21})\left(\frac{n_1}{n_2}\right)^2 \quad (C.11)$$

$$H(\mu) = 1-\rho_{23}\rho_{21}E_2(2d_2) \quad (C.12)$$

$$n_{ij} = \frac{n_i}{n_j} \quad (C.13)$$

$$J = H(1-\rho_{12}\rho_{10}E_1(2d_1))-\rho_{23}\rho_{10}(1-\rho_{12})(1-\rho_{21})E_1(2d_1)E_2(2d_2) \quad (C.14)$$

References

[1] Modest MF, Zhang H. The full-spectrum correlated-k distribution for thermal radiation from molecular gas-particulate mixtures. J Heat Transf 2002;124(1):30–8.
[2] Wang C, He B, Modest MF. Full-spectrum correlated-k-distribution look-up table for radiative transfer in nonhomogeneous participating media with gas–particle mixtures. Int J Heat Mass Transf 2019;137:1053–63.
[3] Denison MK, Webb BW. A spectral line-based weighted-sum-of-gray-gases model for arbitrary RTE solvers. J Heat Transf 1993;115(4):1004–12.
[4] Solovjov VP, Andre F, Lemonnier D, Webb BW. The rank correlated SLW model of gas radiation in non-uniform media. J Quant Spectrosc Radiat Transf 2017;197:26–44.
[5] Modest MF. The weighted-sum-of-gray-gases model for arbitrary solution methods in radiative transfer. J Heat Transf 1991;113(3):650–6.
[6] Bordbar H, Fraga GC, Hostikka S. An extended weighted-sum-of-gray-gases model to account for all CO_2-H_2O molar fraction ratios in thermal radiation. Int Commun Heat and Mass Transf 2020;110:104400.
[7] Bordbar MH, Wecel G, Hyppänen T. A line by line based weighted sum of gray gases model for inhomogeneous CO_2–H_2O mixture in oxy-fired combustion. Combust flame 2014;161(9):2435–45.
[8] Bordbar H, Coelho FR, Fraga GC, França FHR, Hostikka S. Pressure-dependent weighted-sum-of-gray-gases models for heterogeneous CO_2-H_2O mixtures at sub-and super-atmospheric pressure. Int J Heat Mass Transf 2021;173:121207.
[9] Fiveland WA, Jamaluddin AS. Three-dimensional spectral radiative heat transfer solutions by the discrete-ordinates method. J Thermophys Heat Transf 1991;5(3):335–9.
[10] Guo Z, Kumar S. Three-dimensional discrete ordinates method in transient radiative transfer. J Thermophys Heat Transf 2002;16(3):289–96.
[11] Chai JC, Lee HS, Patankar SV. Finite volume method for radiation heat transfer. J Thermophys Heat Transf 1994;8(3):419–25.
[12] Murthy JY, Mathur SR. Finite volume method for radiative heat transfer using unstructured meshes. J Thermophys Heat Transf 1998;12(3):313–21.
[13] Modest MF, Lei S. The simplified spherical harmonics method for radiative heat transfer. J Phys: Conf Ser 2012;369:012019. IOP Publishing
[14] Bordbar MH, Hyppänen T. The correlation based zonal method and its application to the back pass channel of oxy/air-fired CFB boiler. Appl Therm Eng 2015;78:351–63. doi:10.1016/j.applthermaleng.2014.12.046.
[15] Bordbar MH, Hyppänen T. Multiscale numerical simulation of radiation heat transfer in participating media. Heat Transf Eng 2013;34:54–69. doi:10.1080/01457632.2013.695210.
[16] Radice D, Abdikamalov E, Rezzolla L, Ott CD. A new spherical harmonics scheme for multi-dimensional radiation transport i. static matter configurations. J Comput Phys 2013;242:648–69.
[17] Isojärvi T, Bordbar H, Hostikka S. Spectrally resolved calculation of thermal radiation penetration into liquid n-heptane in pool fires. Int J Heat Mass Transf 2018;127:1101–9.
[18] Alinejad F, Bordbar H, Hostikka S. Development of full spectrum correlated k–model for spectral radiation penetration within liquid fuels. Int J Heat Mass Transf 2020;158:119990.
[19] Ottaviani M, Chowdhary J, Cairns B. Remote sensing of the ocean surface refractive index via short-wave infrared polarimetry. Remote Sens Environ 2019;221:14–23.
[20] Ma Y, Luo X. Two-dimensional axisymmetric opto-thermal phosphor modeling based on fluorescent radiative transfer equation. J Lumin 2019;214:116589.
[21] Kumar V, Shrivastava RL, Untawale SP. Fresnel lens: a promising alternative of reflectors in concentrated solar power. Renew Sustain Energy Rev 2015;44:376–90.
[22] Leino AA, Pulkkinen A, Tarvainen T. ValoMC: a Monte Carlo software and MATLAB toolbox for simulating light transport in biological tissue. OSA Contin 2019;2(3):957–72.
[23] Rozenbaum O, Blanchard C, De Sousa MD. Determination of high-temperature radiative properties of porous silica by combined image analysis, infrared spectroscopy and numerical simulation. Int J Therm Sci 2019;137:552–9.
[24] Liu J, Zhang SJ, Chen YS. Modeling of radiative transfer in optical fiber drawing processes with fresnel interfaces. Numer Heat Transf: Part B: Fund 2001;39(4):345–70.
[25] Zhang Y, Zhou P-C, Ma Y, Yi H-L, Tan H-P. Transient radiative transfer in a graded index slab with fresnel surfaces. J Thermophys Heat Transf 2016:513–22.
[26] Modest MF. Radiative heat transfer. 3rd. Academic Press; 2013.
[27] Dombrovsky L, Randrianalisoa J, Baillis D. Modified two-flux approximation for identification of radiative properties of absorbing and scattering media from directional-hemispherical measurements. JOSA A 2006;23(1):91–8.
[28] Liou B-T, Wu C-Y. Composite discrete-ordinate solutions for radiative transfer in a two-layer medium with fresnel interfaces. Numer Heat Transf, Part A Appl 1996;30(7):739–51.
[29] Zhang L, Zhao JM, Liu LH. Finite element approach for radiative transfer in multi-layer graded index cylindrical medium with fresnel surfaces. J Quant Spectrosc Radiat Transf 2010;111(3):420–32.
[30] Wei L, Qi H, Sun J, Ren Y, Ruan L. Spectral collocation method with a flexible angular discretization scheme for radiative transfer in multi-layer graded index medium. Infrared Phys Technol 2017;82:144–53.
[31] Zhang Y, Xie X-Q, Yi H-L, Zhu J-Q. Analysis of radiative heat transfer in two-dimensional semitransparent medium with piece-wise constant refractive index. Int J Heat Mass Transf 2017;115:482–7.
[32] Le Hardy D, Favennec Y, Rousseau B. Solution of the 2-D steady-state radiative transfer equation in participating media with specular reflections using SUPG and DG finite elements. J Quant Spectrosc Radiat Transf 2016;179:149–64.
[33] Murthy JY, Mathur SR. A finite-volume scheme for radiative heat transfer in semitransparent media. Numer Heat Transf: Part B: Fund 2000;37(1):25–43.
[34] Mengüç MP, Viskanta R. Comparison of radiative transfer approximations for a highly forward scattering planar medium. J Quant Spectrosc Radiat Transf 1983;29(5):381–94.
[35] Elghazaly A, El-Konsol S, Sabbah AS, Hosni M. Anisotropic radiation transfer in a two-layer inhomogeneous slab with reflecting boundaries. Int J Therm Sci 2017;120:148–61.
[36] Jinbo H, Liming R, Heping T. Effect of anisotropic scattering on radiative heat transfer in two-dimensional rectangular media. J Quant Spectrosc Radiat Transf 2003;78(2):151–61.
[37] Boulet P, Collin A, Consalvi JL. On the finite volume method and the discrete ordinates method regarding radiative heat transfer in acute forward anisotropic scattering media. J Quant Spectrosc Radiat Transf 2007;104(3):460–73.
[38] Chai J, Lee HS, Patankar SV. Improved treatment of scattering using the discrete ordinates method. J Heat Transf 1994;116(1):260–3.
[39] Bordbar H, Hyppänen T. Line by line based band identification for non-gray gas modeling with a banded approach. Int J Heat Mass Transf 2018;127:870–84.
[40] Atkinson K, Han W. Numerical solution of Fredholm integral equations of the second kind. In: Theoretical numerical analysis. Springer; 2009. p. 473–549.
[41] Wu C-Y, Bo-Ting L. Radiative transfer in a two-layer slab with fresnel interfaces. J Quant Spectrosc Radiat Transf 1996;56(4):573–89.
[42] McGrattan KB, Hostikka S, Floyd JE, McDermott R, Vanella M. Fire dynamics simulator – technical reference guide. National Institute of Standards and Technology, Building and Fire Research Laboratory; 2020.